Supporting Information

$Ti_3C_2T_x$ MXene - embedded MnO_2-based hydrophilic electrospun carbon nanofibers as a freestanding electrode for supercapacitors

Zhaorui Wang [1], Deyang Zhang [1*], Ying Guo [1], Hao Jiang [2], Di Wang [1], Jinbing Cheng [2*], Paul K. Chu [3], Hailong Yan [1], Yongsong Luo [1,2*]

[1] Henan Joint International Research Laboratory of New Energy Storage Technology, Xinyang Normal University, Xinyang 464000, P. R. China

[2] College of Physics and Electronic Engineering, Nanyang Normal University, Nanyang 473061, P. R. China

[3] Department of Physics, Department of Materials Science & Engineering, and Department of Biomedical Engineering, City University of Hong Kong, Tat Chee Avenue, Kowloon, Hong Kong, China

Experimental Section

Materials

The Ti_3AlC_2 powder (400 mesh) was purchased from Enwang New Materials Technology Co., Ltd. and manganese acetate tetrahydrate ($Mn(CH_3COO)_2•4H_2O$, 99%), anhydrous sodium sulfate (Na_2SO_4, ≥99.0%), N, N-dimethyl formamide (DMF, 99.9%), and polyacrylonitrile (PAN, Mw = 150,000) were provided by Aladdin. All the reagents were analytical grade and used without further purification.

Synthesis of $Ti_3C_2T_x$ MXene

The $Ti_3C_2T_x$ nanosheets were produced by LiF/HCl etching and exfoliation Ti_3AlC_2. Typically, LiF (1 g) was added to 30 ml of 9 mol/L hydrochloric acid and heated to 36℃ during stirring. 5 ml of 40% HF were added when the solution became clear and after 1 g of Ti_3AlC_2 MAX was added, the reaction proceeded for 12 h. The black solution was washed repeatedly with deionized water and centrifuged at 5,000 rpm until the pH ≥ 6. The dark green mud deposit was collected and transferred to a bottle under Ar atmosphere and sonicated under Ar for an hour. It was washed repeatedly with deionized water and centrifuged at 10,000 rpm to collect the product. To obtain the solution for electrospinning, the product obtained from the previous step was washed three times with DMF, and the concentration was adjusted to 20 mg mL^{-1}.

Synthesis of $Ti_3C_2T_x$/CNFs

The $Ti_3C_2T_x$/CNFs were synthesized by electrospinning, pre-oxidation, and carbonization. In brief, polyacrylonitrile (0.65 g) was dispersed in 5 ml of the $Ti_3C_2T_x$ solution, stirred continuously for 6 h, and placed in a 5 mL plastic syringe with an 18 G blunt-tip needle. A positive voltage (20 kV) was applied to the needle tip and the copper collector roller covered by an aluminum foil was grounded. The distance between the needle tip and collector was 12 cm, and the infusion rate of the solution was 0.8 mL h^{-1}. The samples were electrospun at a relative humidity below 30%. The electrospun mats were first stabilized in air at 267 ℃ for 2 h at a ramping rate of 3 ℃ min^{-1} and then carbonized under argon at a ramping rate of 2 ℃ min^{-1} at 800 ℃ for up to 2 h.

Synthesis of MnO_2@ $Ti_3C_2T_x$ /CNFs

MnO_2 nanosheets were prepared by anodic constant current electrodeposition on CH660E electrochemical workstation. Typical, the electrodeposition solution was prepared by adding 6mM manganese acetate and sodium sulfate to 60ml deionized water. Before electrodeposition, a film was weighed as m_1. A three-electrode system was assembled, in which the working electrode was $Ti_3C_2T_x$/CNFs, the pair motor was platinum plate electrode, and the reference electrode was SCE. The anode current was set to 0.0013 mA / cm^2 relative to the film area. The electrodeposition time is set to 350 s. After the electrodeposition, the electrode was washed with deionized water and dried in an oven at 60 °C for 1 hour and weighed as m_2. m_1- m_2 is the active mass for the MnO_2@$Ti_3C_2T_x$/CNFs material. MnO_2@$Ti_3C_2T_x$ and MnO_2@CNFs were

fabricated by the same method. Where $Ti_3C_2T_x$ is obtained by vacuum filtration.

Fabrication of all-solid-state asymmetric supercapacitors

The all-solid-state button asymmetric supercapacitors (ASCs) were assembled with MnO_2@$Ti_3C_2T_x$/CNFs and AC@NC as the positive and negative electrodes, respectively and 1 M Na_2SO_4 as the electrolyte. The specific capacity of activated carbon is 150 F/g. The activated carbon slurry is composed of activated carbon, conductive carbon black and PTFE, and the ratio is 7: 2: 1. In order to ensure the charge balance, the load quality of the cathode should be matched with the anode.

Materials characterization

The crystalline structure and phase of the composites were identified by X-ray diffraction (XRD, Bruker D2 PHASER) using Cu-K_α (λ = 1.5418 Å) radiation at 40 kV, 40 mA, and2θ between 5° and 80° at room temperature. Raman scattering was carried out on the INVIA Raman microprobe (Renishaw Instruments) with a 532 nm laser source and a 50× objective lens at a laser power of 5%. The chemical composition was determined by X-ray photoelectron spectroscopy (XPS, K-ALPHA 0.5 eV) with a resolution of 0.3-0.5 eV using a monochromatic aluminum X-ray source. The morphology was examined by field-emission scanning electron microscopy (SEM, Hitachi S-4800) and transmission electron microscopy (TEM, FEI Tecnai G2 F20) and elemental analysis was carried out by energy-dispersive X-ray spectroscopy (EDS, Bruker QUANTAX) on the TEM.

Electrochemical assessment

The electrochemical properties of MnO_2@CNFs, MnO_2@$Ti_3C_2T_x$, and MnO_2@$Ti_3C_2T_x$/CNFs were determined in 1 M Na_2SO_4 using the traditional three-electrode system at 25 °C. The platinum and saturated calomel electrodes were the counter and reference electrodes, respectively, in the CHI660E electrochemical workstation. The asymmetric supercapacitor was assembled with MnO_2@$Ti_3C_2T_x$/CNFs as the positive electrode, AC as the negative electrode, and PVA/Na_2SO_4 gel electrolyte as the electrolyte.

Cyclic voltammetry (CV) was performed in a voltage window from 0 to 1 V, and the GCD curves were acquired between 0 and 1 V. Electrochemical impedance spectroscopy (EIS) was conducted at frequencies between 0.01 Hz and 100 kHz. The specific capacitance (C_m, F g^{-1}) was calculated by the following equation:

$$C_m = \frac{I \times \Delta t}{m \times \Delta V},$$

where I (A) is the applied current, Δt (s) is the discharging time, ΔV (V) is the discharging potential range, and m (g) is the total mass of active materials. The theoretical pseudo capacitance was calculated as follows:

$$C = \frac{n \times F}{M \times V},$$

where n (mol) is the number of electrons transferred in the redox reaction, M (g. mol^{-1}) is the molar mass of the materials, F (C. mol^{-1}) is Faraday's constant, and V (V) is the operating voltage window, respectively. The charge balance between the two

electrodes should follow the relationship $q^+ = q^-$, where q is the charge stored in the electrode calculated by the following equation:

$$q = C_m \times \Delta E \times m,$$

where Cm (F g^{-1}) is the specific capacitance, ΔE (V) is the potential range in the charging/discharging process, and m (g) is the mass loading of the active materials. The ideal mass ratio of the active materials on the positive (MnO_2@$Ti_3C_2T_x$/CNFs) and the negative electrode (AC) in the asymmetric supercapacitor (m+/m-) was calculated by the equation:

$$\frac{m^+}{m^-} = \frac{\Delta E_- \times C_-}{\Delta E_+ \times C_+}.$$

The energy density (E) and power density (P) were calculated by the following equations:

$$E = \frac{1}{2 \times 3.6} C_m (\Delta E)^2$$ and

$$P = \frac{E \times 3600}{\Delta t},$$

where E (Wh kg^{-1}) is the energy density, C_m (F g^{-1}) is the specific capacitance, ΔV (V) is the operating potential window, P (kW kg^{-1}) is the power density, and Δt(s) is the discharging time.

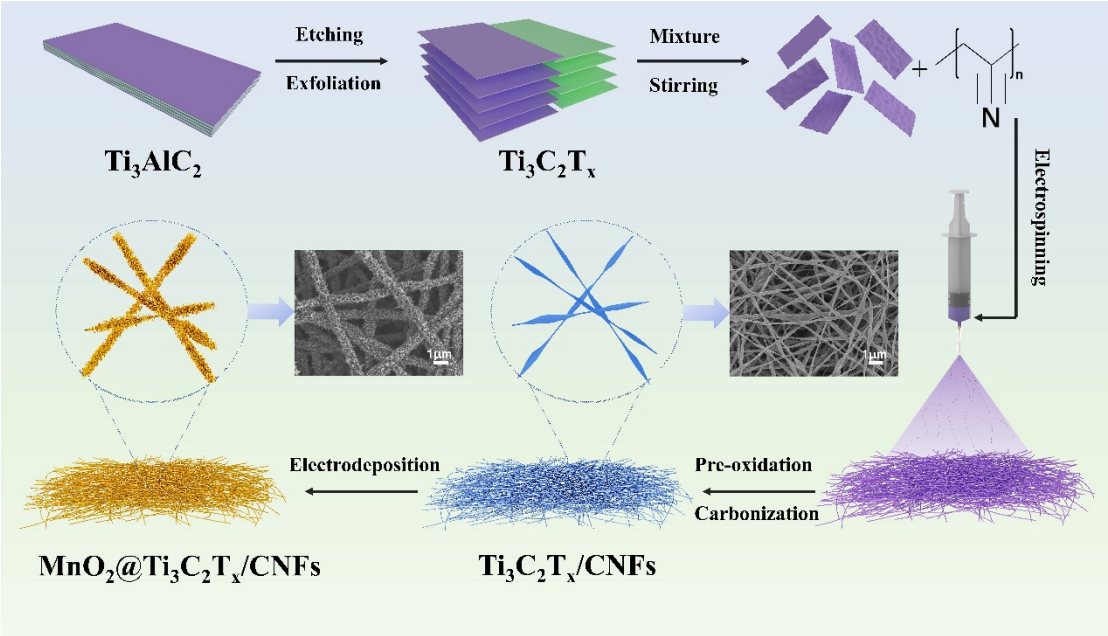

Figure S1. Schematic illustration of the multi-step fabrication procedures of the $MnO_2@Ti_3C_2T_x$/CNFs nanocomposite.

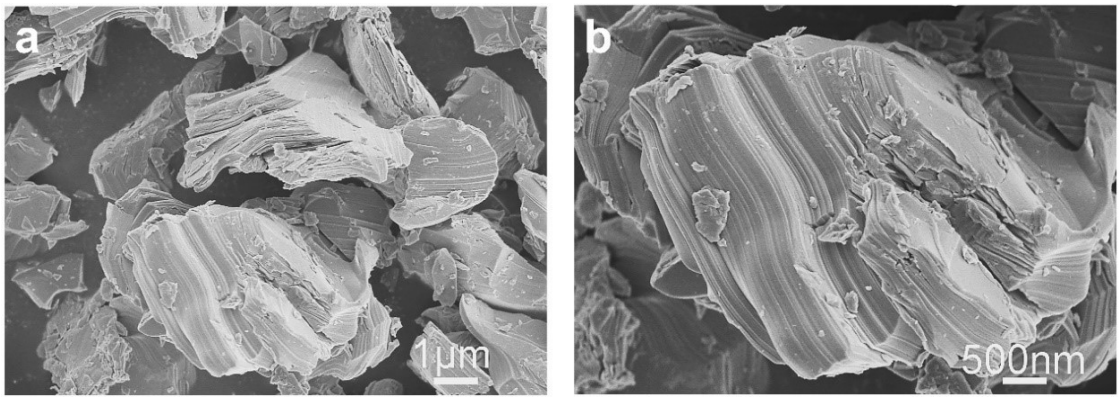

Figure S2. (a-b) SEM images of the Ti_3AlC_2 powders.

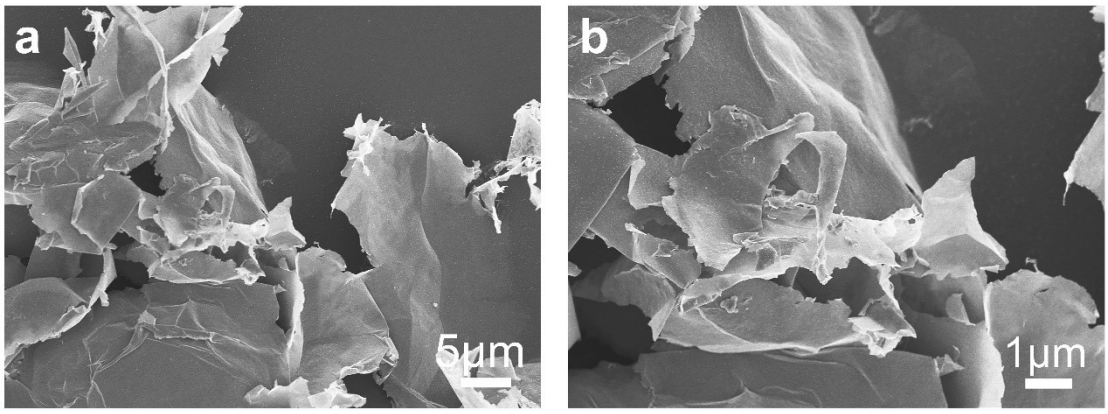

Figure S3. (a-b) SEM images of the $Ti_3C_2T_x$ powders.

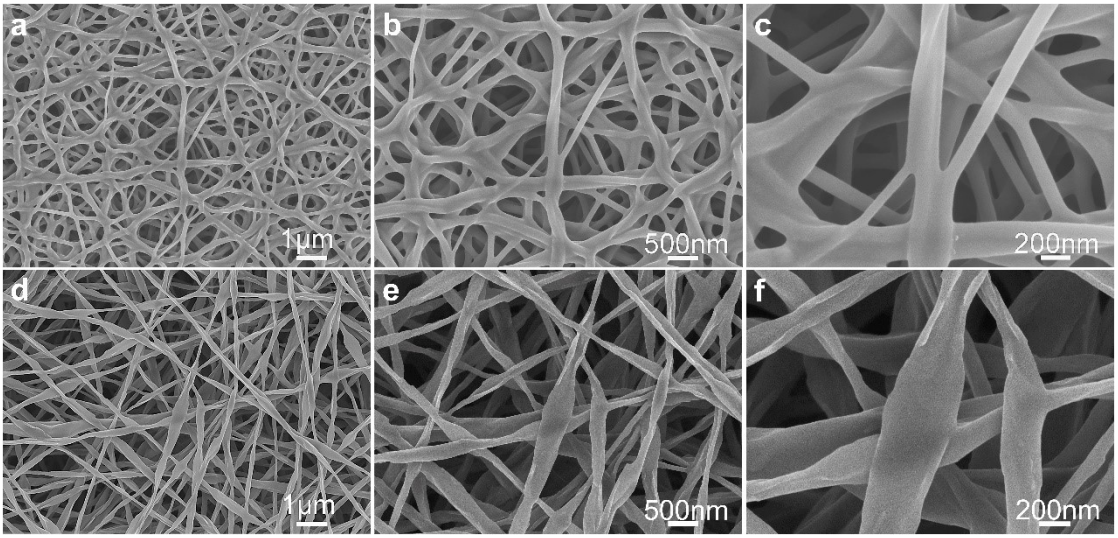

Figure S4.SEM images: (a-b) CNFs and (d-f) $Ti_3C_2T_x$/CNFs.

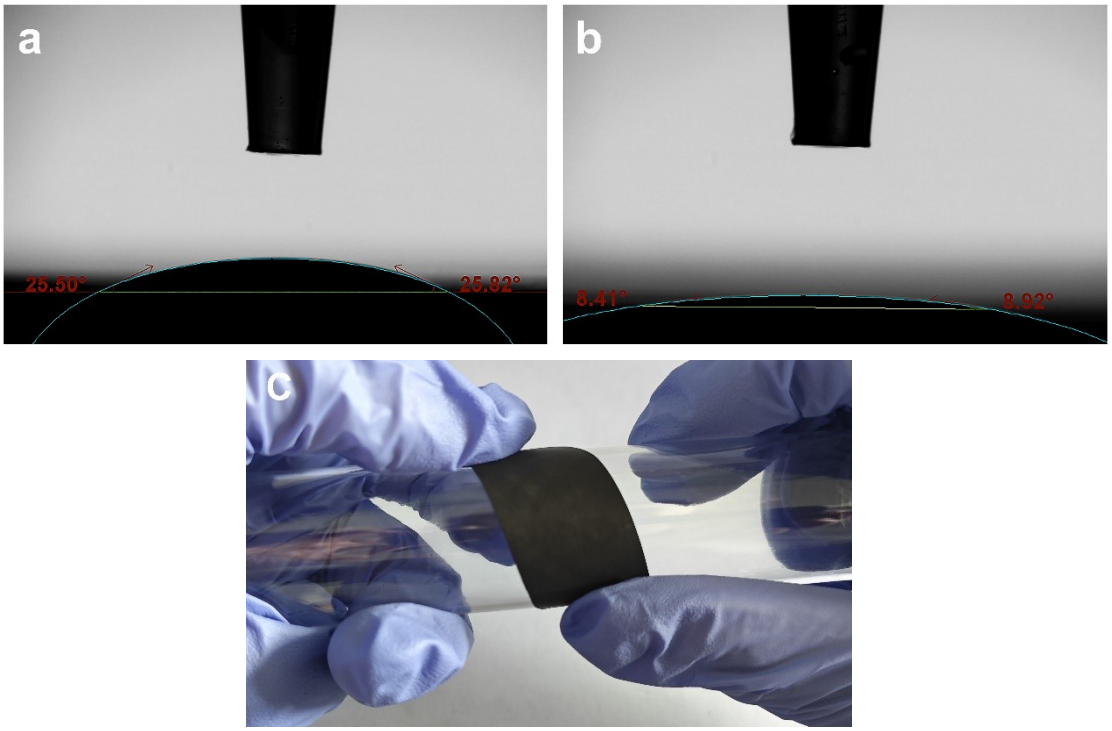

Figure S5. (a-b) Hydrophilicity comparison of CNFs and $Ti_3C_2T_x$/CNFs (Left contact angle of CNFs is 25.5°, right is 25.85°, and mean is 25.66°; Left contact angle of $Ti_3C_2T_x$/CNFs is 8.41°, right is 8.92°, and mean is 8.67°; (c) Flexibility of the thin film.

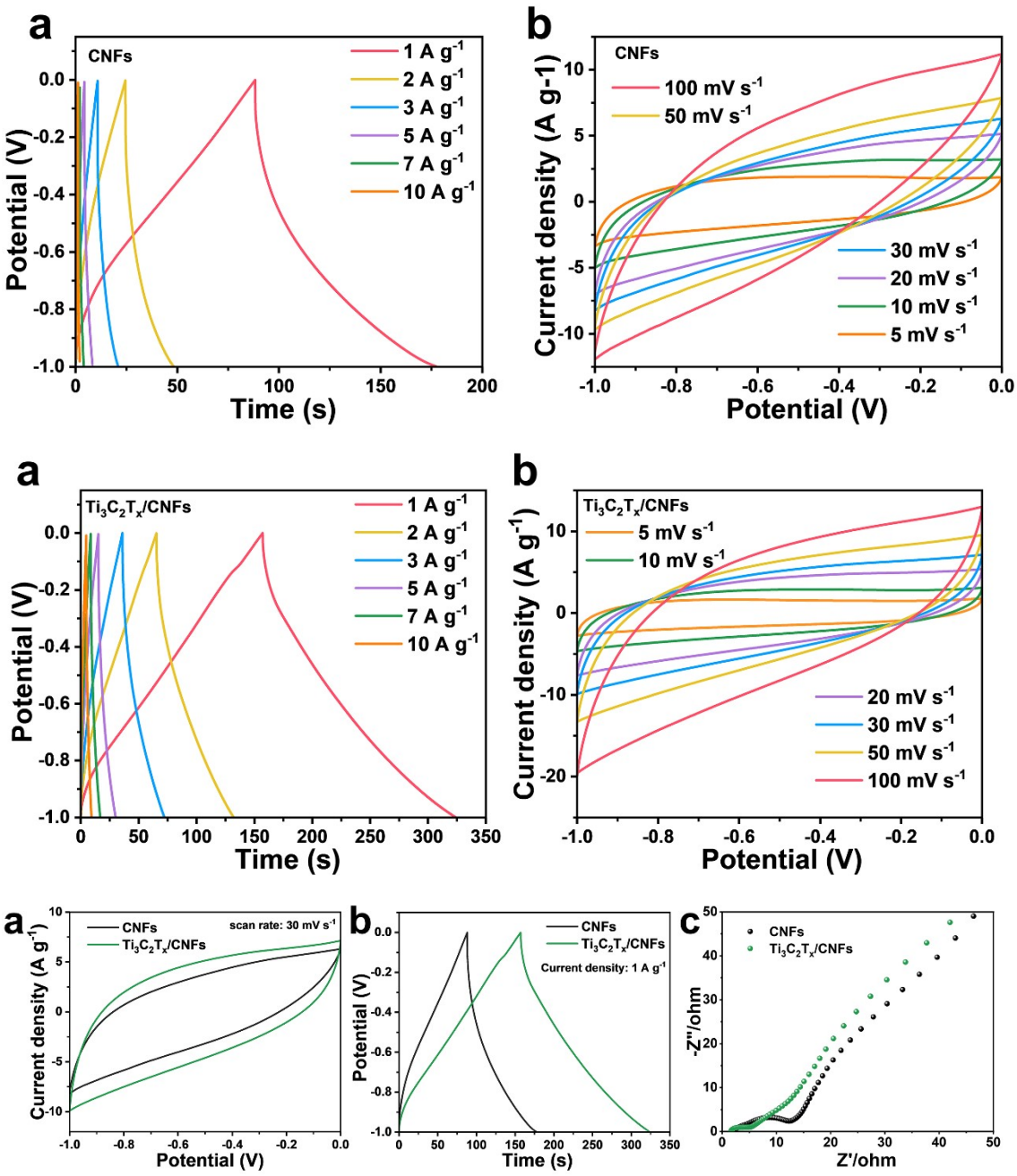

Figure S6. The electrochemical characterization of CNFs and $Ti_3C_2T_x$/CNFs self-supported electrode. The capability of CNFs are 88.2, 47.6, 30.3, 20, 13.3, and 8 F g^{-1} at current densities of 1, 2, 3, 5 7, and 10, respectively. The capability of $Ti_3C_2T_x$/CNFs are 166.9, 133.2, 109.2, 75, 57.4, and 44 F g^{-1} at current densities of 1, 2, 3, 5 7, and 10, respectively. The impedance diagram also shows that the semicircle part of $Ti_3C_2T_x$/CNFs is significantly smaller than that of CNFs. Whether at the same scanning

rate or current density or impedance diagram, the $Ti_3C_2T_x$/CNFs is better than CNFs.

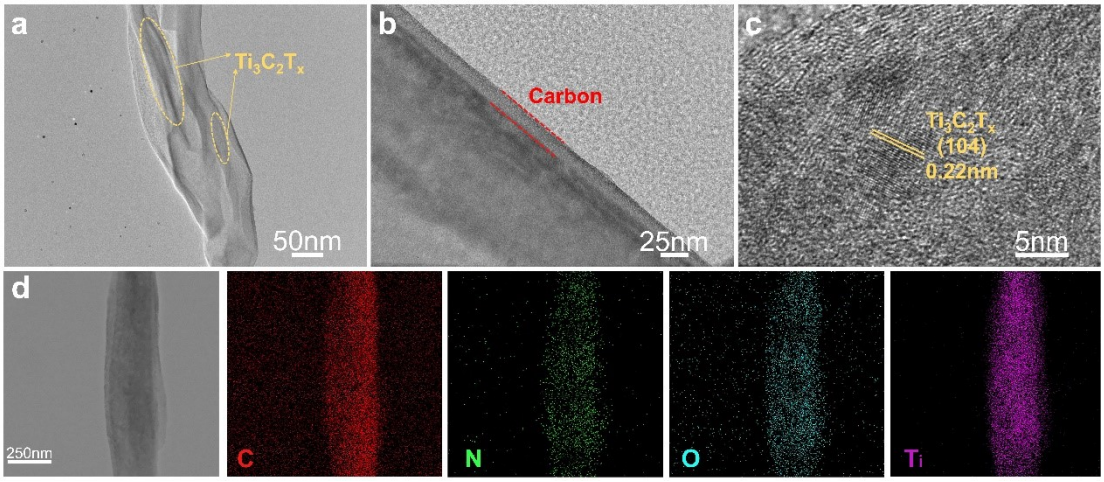

Figure S7. (a-c) TEM images of $Ti_3C_2T_x$/CNFs fibers and (d) Elemental maps of $Ti_3C_2T_x$/CNFs.

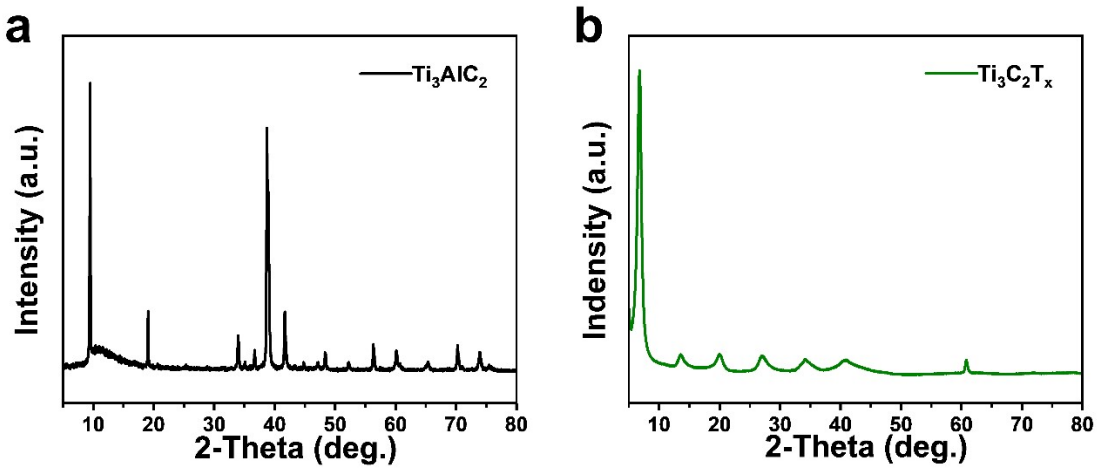

Figure S8. XRD patterns of (a) Ti_3AlC_2 and (b) $Ti_3C_2T_x$.

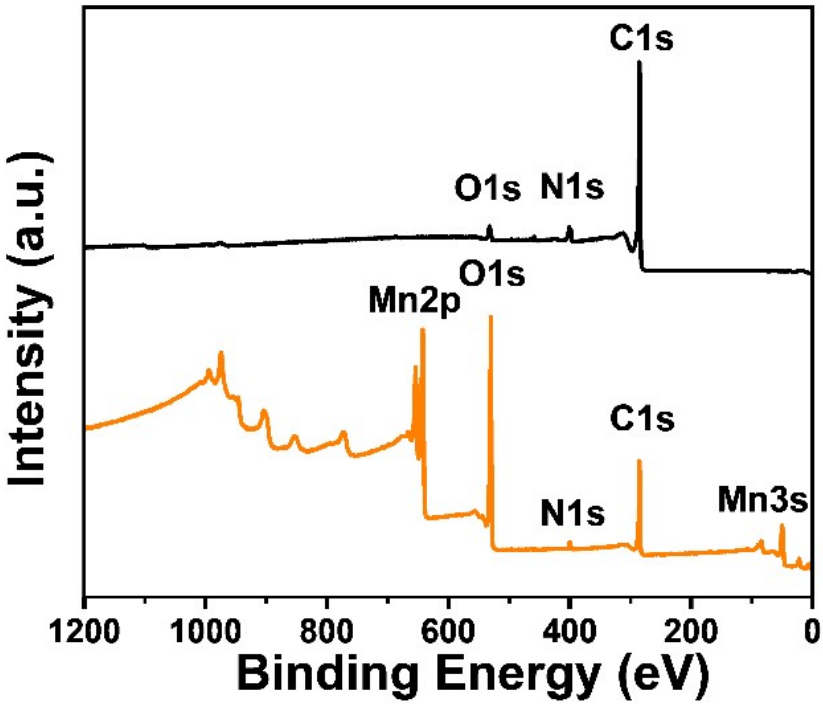

Figure S9. XPS survey spectra of $Ti_3C_2T_x$/CNFs and MnO_2@$Ti_3C_2T_x$/CNFs.

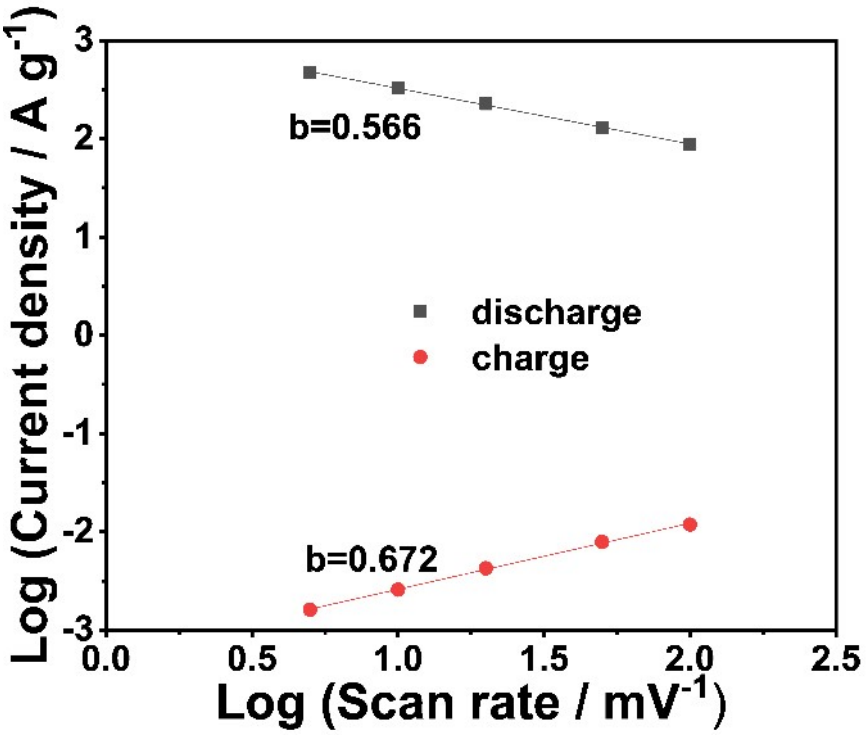

Figure S10 a. Fitted linear curves of log *i* versus log *v* based on the CV results.

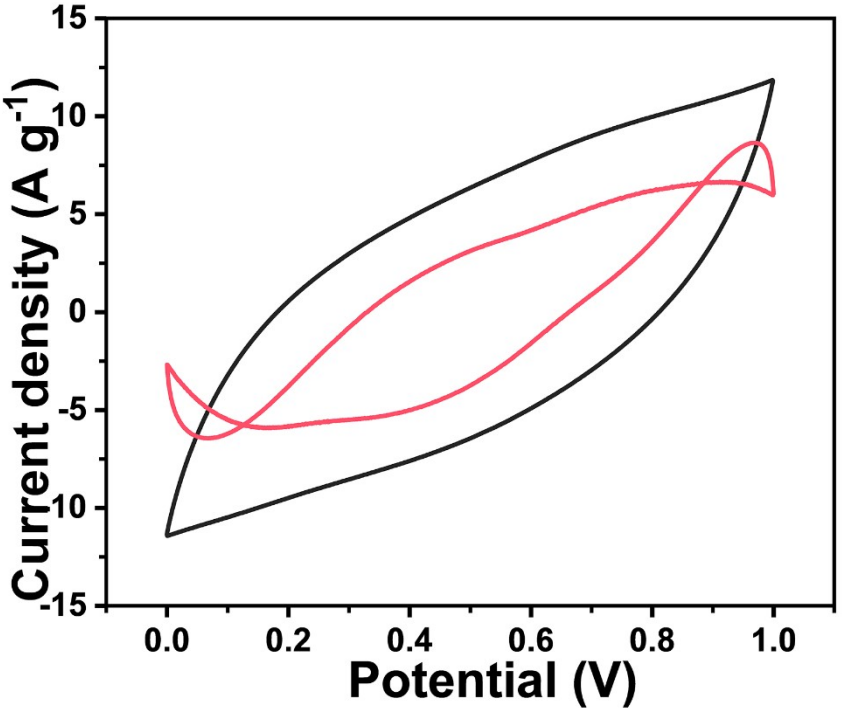

Figure S10 b. The surface-controlled processes account for capacitance contribution of MnO_2@$Ti_3C_2T_x$/CNFs is 67.7% of the total capacitance in 100 mV s^{-1}.

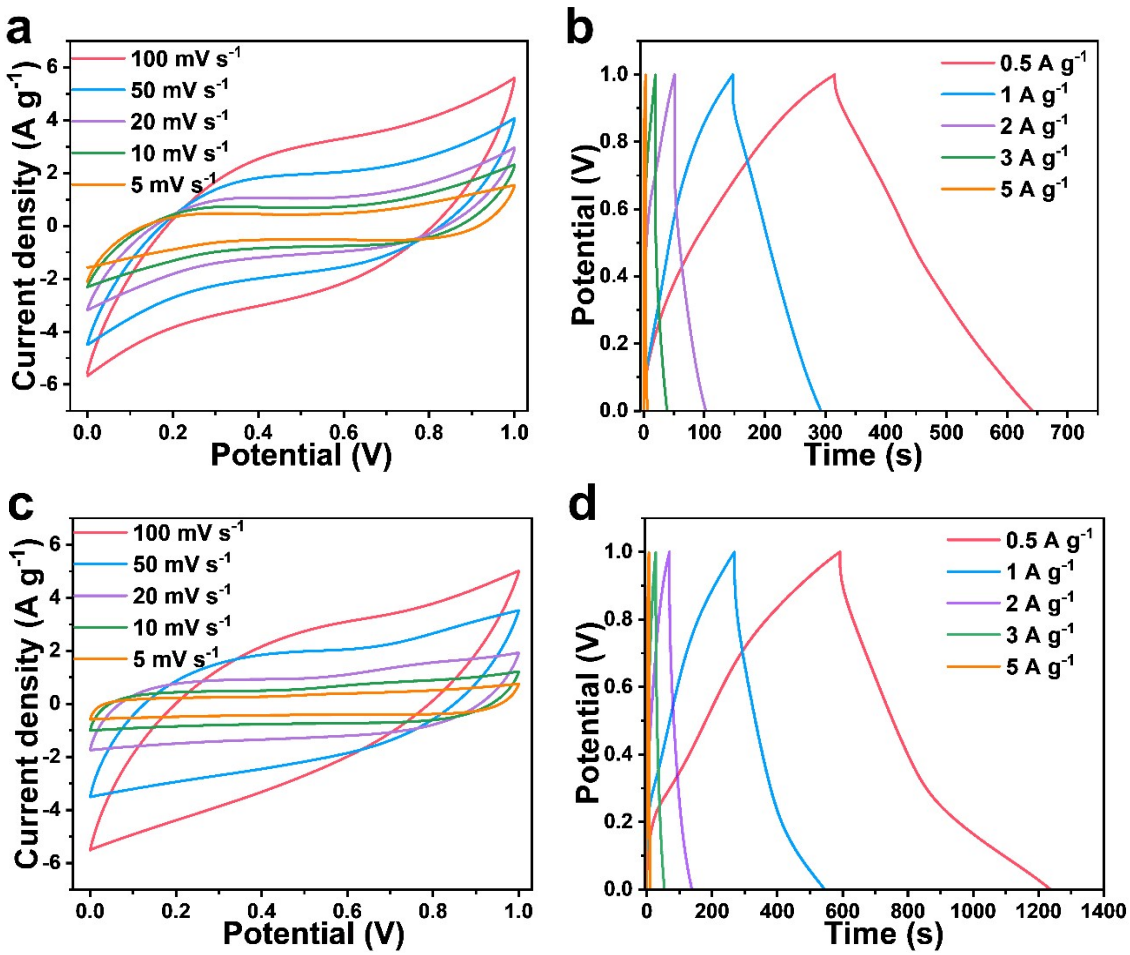

Figure S11. MnO_2@$Ti_3C_2T_x$: (a) CV curves and (b) GCD plots; MnO_2@CNFs: (c) CV curves and (d) GCD plots.

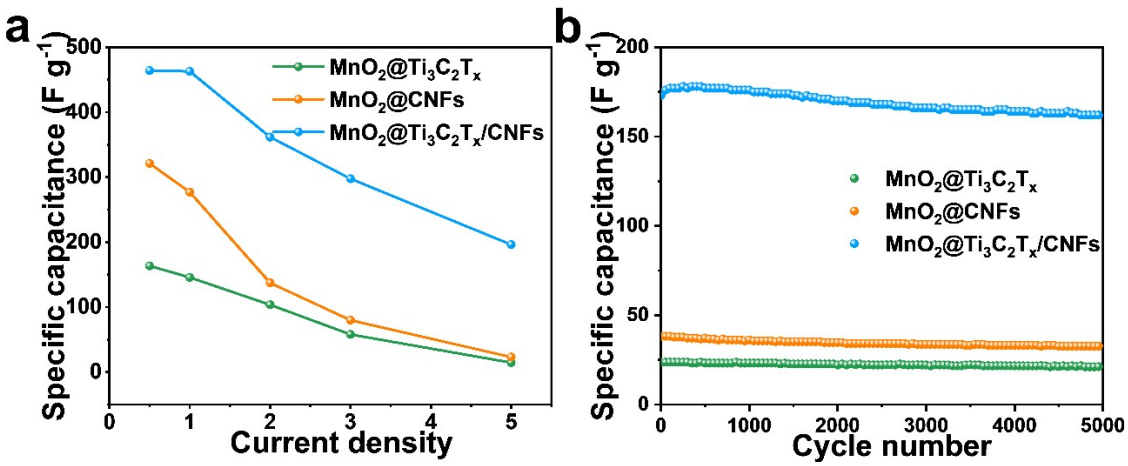

Figure S12. (a) Capacitances of $MnO_2@Ti_3C_2T_x$, MnO_2@CNFs, and $MnO_2@Ti_3C_2T_x$/CNFs for different current densities and (b) Cycling stability of $MnO_2@Ti_3C_2T_x$, MnO_2@CNFs, and $MnO_2@Ti_3C_2T_x$/CNFs.

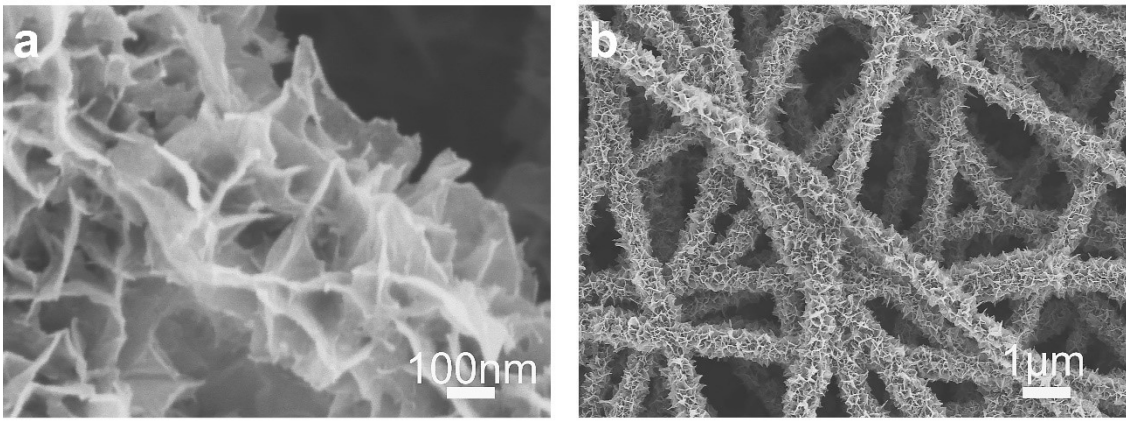

Figure S13 a. SEM images of MnO_2@$Ti_3C_2T_x$/CNFs electrode after 5,000 cycles.

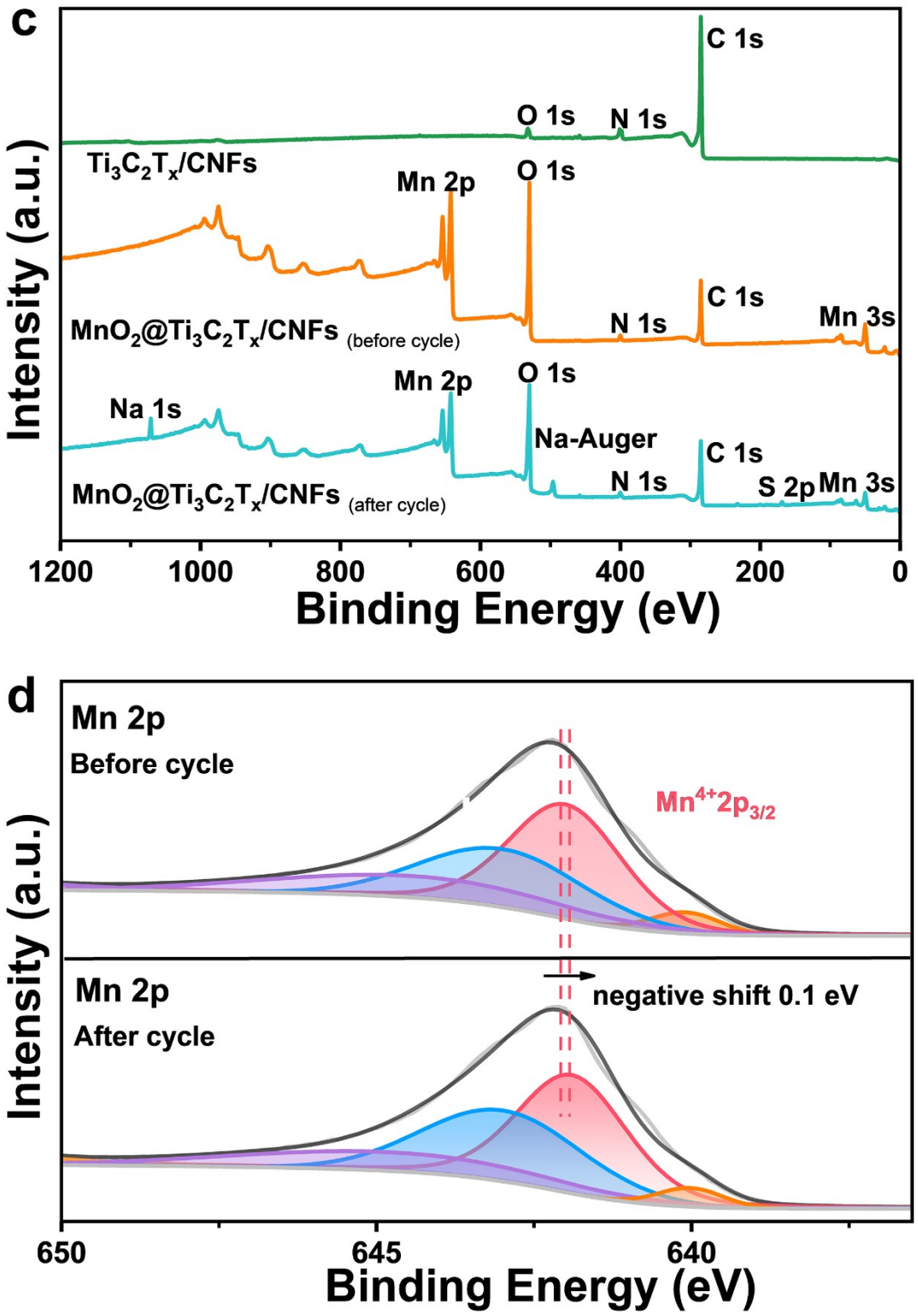

Figure S13 c&d. XPS comparison of MnO_2@$Ti_3C_2T_x$/CNFs electrode before and after 5,000 cycles. Due to the intercalation of Na^+, the elemental peak of Na can be seen in the XPS spectrum after the cycle, while there is no corresponding part of the spectrum

before the cycle (Figure S13c). Figure S13 d shows the refinement of Mn element. It can be seen that the main peak of Mn^{4+} shifts to the low binding energy which corresponds to the decrease of the valence state of Mn caused by Na^+ intercalation.

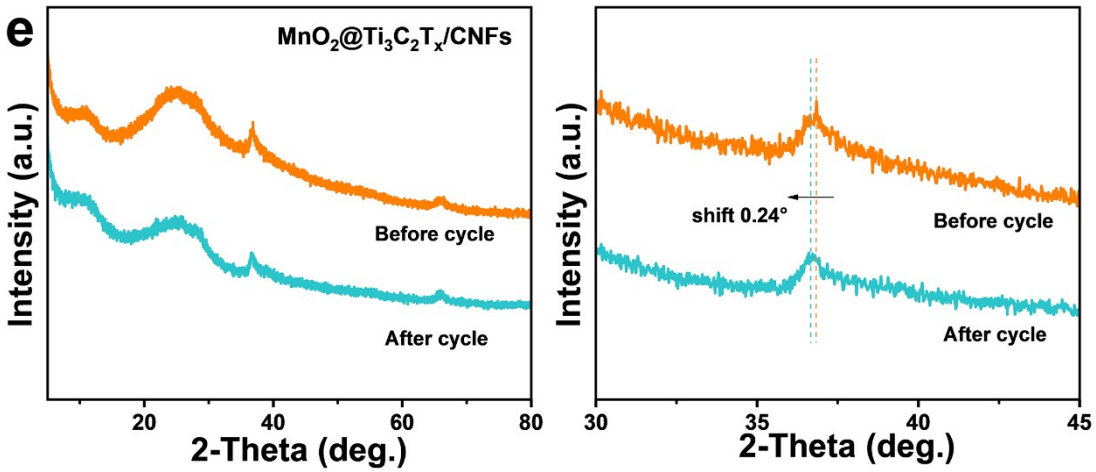

Figure S13 e. XRD comparison of MnO_2@$Ti_3C_2T_x$/CNFs electrode before and after 5,000 cycles. The XRD of the material before and after the cycle also showed a small peak shift. This corresponds to the increase of interlayer spacing of MnO_2 caused by Na^+ intercalation.

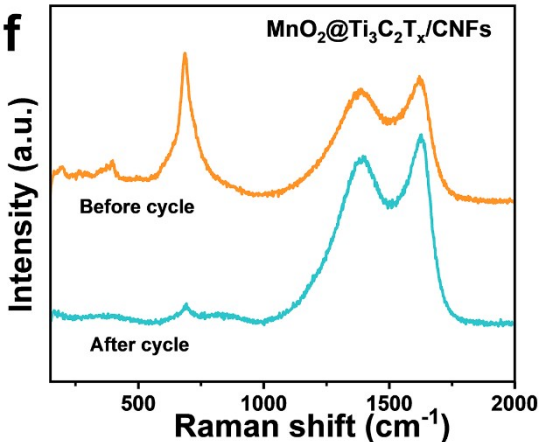

Figure S13 f. Raman comparison of MnO_2@$Ti_3C_2T_x$/CNFs electrode before and after 5,000 cycles. The Raman spectra of the material before and after cycling show the

decrease of Mn signal and the enhancement of D and G peaks, which may be caused by the increase of carbon fiber signal caused by partial dissolution of MnO_2.

Materials	Energy density (W h kg^{-1})	Power density （kW kg^{-1}）	Cycling stability	Reference
MnO_2@$Ti_3C_2T_x$/CNFs//AC	46.4	0.4	5000c/83%	This work
0.5-CNT@MnO_2/CFC//AC/CFC	27.8	0.25	10000c/84%	1
MnO_2/p- $Ti_3C_2T_x$//$Ti_3C_2T_x$	14.3	0.79	2000c/80%	2
CoB-V-MX//AC	31.5	0.8	2500c/89.2%	3
$Ti_3C_2T_x$/CuS//$Ti_3C_2T_x$	15.4	0.75	5000c/82.4%	4
1 T-VS_2-MX // $Ti_3C_2T_x$	41.13	0.793	5000c/85%	5
MXene-PPy//MnO2	26.7	0.32	5000c/86.9%	6
NZ-R-2-200/K-Ar-MXene// NPC/rGO	57.48	0.4	2000c/60%	7

Table S1. The performance of this work is compared with that of ASC devices with similar work recently.

Equation S1:

$$(MnO_2)_{suface} + M^+ + e^+ = (MnOOH)_{sufaces}$$

And

$$(MnO_2)_{bulk} + M^+ + e^+ = (MnOOH)_{bulk},$$

where M^+ is related to H^+ or alkali metal cations such as Li^+, Na^+, or K^+. The first equation represents surface adsorption and desorption of protons or alkali metal ions, while the second equation indicates bulk insertion and extraction of these ions. In the two-step reversible redox reaction, the oxidation states of Mn ions change between III and IV.

Equation S2:

$i = aV^b$

If the value of the constant b is 1, the charge storage is predominantly influenced by surface processes. Conversely, when the value of b is 0.5, charge storage is primarily governed by diffusion processes.

Equation S3:

$$I(V) = k_1 V + k_2 V^{1/2}$$

The first term on the right side of the equation corresponds to the capacitance-controlled effect and the other involves diffusion-controlled insertion. i(V) and v are the current at potential V and scanning rate, slope, and intercept by plotting $i(V)/v^{1/2}$ against $v^{1/2}$

Refence

1. K. Wu, Z. Ye, Y. Ding, Z. Zhu, X. Peng, D. Li and G. Ma, *Journal of Power Sources*, 2020, **477**.
2. X. Zhang, B. Shao, A. Guo, Z. Sun, J. Zhao, F. Cui and X. Yang, *Applied Surface Science*, 2021, **560**.
3. R. Venkatkarthick, J. Qin and T. Maiyalagan, International Journal of Energy Research, 2022, 46, 22474-22485.
4. Z. Pan, F. Cao, X. Hu and X. Ji, Journal of Materials Chemistry A, 2019, 7, 8984-8992.
5. Sharma A, Mane P and Chakraborty B, Rout CS. ACS Appl Energy Mater. 2021;4(12):14198-14209.
6. R. A. Chavan and A. V. Ghule, Nanotechnology, 2023, 34.
7. A. Ganiyat Olatoye, W. Li, E. Oluwaseyi Fagbohun, X. Zeng, Y. Zheng and Y. Cui, Journal of Electroanalytical Chemistry, 2023, 928.